

# Estimating Induction Motor State Based on Current Signals in the Conditions of Limited Data Set Using Recurring Images

A. L. Shestakov<sup>\*,a</sup>, D. V. Galyshev<sup>\*,b</sup>, O. L. Ibryaeva<sup>\*,c</sup>, and V. A. Ereemeeva<sup>\*,d</sup>

<sup>\*</sup>South Ural State University, Chelyabinsk, Russia

e-mail: <sup>a</sup>a.l.shestakov@susu.ru, <sup>b</sup>galyshevdv@susu.ru, <sup>c</sup>ibryaevaol@susu.ru, <sup>d</sup>eremeeva@susu.ru

Received May 20, 2024

Revised June 20, 2024

Accepted July 23, 2024

**Abstract**—The paper examines the diagnostics of rotor bar breakage in induction motors using electric current signals in the conditions of limited data set. The available failure detection procedure is based on the filtering of the current around the seventh harmonic of the supply voltage frequency with subsequent development of an envelope underlying the scalograms. Instead of scalograms, the paper offers recurrent graphs, which demonstrate higher computational efficiency. It also proposes the modeling of the lacking abnormal operation data that is typical for real-life operating conditions. The paper shows that a convolutional neural network (CNN) model taught on both design operation data obtained at various operation modes and the abnormal operation data from a single mode poorly detects the defect in case of operation mode changes. This is caused by the change of specific defect frequencies dependent on the operation mode. To overcome this challenge, the paper offers a data augmentation method based on spectrum restructuring. The spectrum of a real-life defective signal is reshaped in view of its structure, and synthetic data are developed, which simulate the lacking defect signals for other operation modes. Experimental testing showed that data augmentation based on spectrum reshaping significantly improves CNN model performance under insufficient volume of defect-mode training data.

*Keywords:* induction motor, broken rotor bar, scalogram, convolutional neural network, recurrent graphs, spectrum reshaping, Hilbert transform, data augmentation

**DOI:** 10.31857/S0005117925050096

## 1. INTRODUCTION

Lifecycle management of industrial equipment is critical for maintaining uninterrupted production processes [1]. Unplanned downtime due to equipment failures results in substantial financial losses, driving modern lifecycle strategies to prioritize machinery condition assessment. This is achieved through specialized monitoring systems that employ data processing algorithms, utilizing measurements from onboard sensors [2]. Integrating advanced analytics into existing monitoring infrastructure allows enterprises to not only improve operational safety but also optimize the performance of complex industrial systems [3].

Induction motors are among the most widespread and mission-critical industrial assets, serving as the primary driving force for the majority of industrial machinery across virtually all manufacturing sectors. However, like all electromechanical equipment, they are susceptible to various operational faults and failures. For instance, a broken rotor bar accounts for up to 10% of all failures in induction motors [4]. Early detection of this fault is crucial, as operating a motor with this defect leads to increased energy consumption, reduced torque output, and elevates the risks of rotor locking and stator winding damage [5].

Most existing diagnostic methods are based on the analysis of side harmonics arising near the power supply frequency  $f_s$ , the amplitude of which increases as the defect progresses [6]:

$$s_{sidepeaks} = (1 \pm 2s)f_s. \quad (1)$$

Here  $s$  is the motor slip. Although side harmonics are an established sign of broken bars, their amplitude may be reduced and masked by the fundamental frequency of the supply voltage, particularly during low-load operation. Partial bar failures further exacerbate this challenge by producing extremely weak diagnostic signals that are prone to noise contamination. Moreover, various operational factors interfere with reliable harmonic detection [7]. Specifically, cyclostationary loads, magnetic asymmetry, and rotor ventilation ducts generate current harmonics in the same spectral range as bar breakage signatures. These confounding factors substantially degrade the diagnostic reliability of conventional harmonic analysis, limiting its effectiveness for precise fault detection.

An alternative diagnostic approach that circumvents these masking effects involves analyzing the motor's starting current transient [8]. This method enables precise fault detection by identifying distinctive time-frequency patterns generated during motor startup. Unlike steady-state operation under cyclostationary loads, the startup transient produces a unique spectral signature that effectively isolates fault-related components from interfering harmonics, significantly improving diagnostic reliability.

However, this diagnostic approach has several important limitations. First, it cannot be applied to motors driven by frequency converters, as their low slip values prevent effective testing. Second, the method is impractical for medium- and high-power motors [9], since implementation requires repeated start-stop cycles that may compromise motor performance and operational efficiency.

When a rotor bar defect occurs, in addition to peaks (1), a number of components in the higher harmonics range also appear in the current signal spectrum [10]:

$$\begin{aligned} f_{space} &= (k(1-s) \pm s)f_s, \\ f_{rotare} &= (k \pm 2ns)f_s, \end{aligned}$$

where  $k = 5, 7$ ,  $n = 1, 2, 3$ . While cyclostationary loads may still obscure certain frequency components in this range, their masking effect is significantly less pronounced compared to the interference observed near the supply frequency's sidebands. Consequently, higher harmonic analysis of the stator current spectrum offers superior diagnostic reliability. For this study, we specifically examine signal characteristics surrounding the seventh harmonic of the supply frequency.

Beyond signal processing challenges, significant obstacles emerge during data acquisition. The development of robust fault diagnosis systems is hindered by the scarcity of failure data, as induction motors typically operate reliably for extended periods with infrequent malfunctions. This scarcity makes it particularly difficult to collect comprehensive datasets encompassing all potential operating conditions. Consequently, the resulting training data often lacks representativeness, posing substantial challenges for building reliable machine learning models capable of generalizing across diverse operational scenarios.

This paper presents a novel diagnostic method for detecting broken rotor bars in induction motors under conditions of severely limited failure data. To address the data scarcity challenge, we introduce an innovative spectrum restructuring technique for signal augmentation that preserves the inherent structure of motor current signatures. The proposed approach combines: (1) advanced analysis of higher-order harmonics in stator current signals with (2) synthetic data generation through physics-informed spectrum transformation. This dual methodology enables reliable fault detection even when training data is sparse or unrepresentative of all operational conditions. Signals are acquired from both healthy and faulty motors under varying load conditions. Each signal is filtered to extract the informative component that exhibits changes in the presence of defects. The faulty signals are then augmented to simulate modes with insufficient load. The processed signals

are then transformed into recurrent graph images and used to train a convolutional neural network (CNN) classifier. During training, the CNN is exposed to defect data from only a single load level, while during testing, it evaluates data across all load conditions. This approach validates the rotor bar break diagnosis model's capability to detect faults under varying motor operating conditions.

The paper is structured as follows: Section 2 presents the proposed diagnostic methodology. Section 3 introduces the spectrum restructuring-based augmentation technique. The experiment is described in Section 4, followed by the discussion of diagnostic model test results in Section 5. The key contribution of this work is demonstrating the efficacy of envelope spectrum distortion-based augmentation when training a classification model using higher-order stator current spatial harmonics as diagnostic features for detecting broken rotor bars in induction motors.

## 2. THE PROPOSED DIAGNOSTIC METHOD

Figure 1 shows the scheme of the broken rotor bar diagnostic method using stator current analysis, used in [11]. The process begins with signal preprocessing, which includes bandpass filtering around the seventh harmonic of the supply frequency. The defect frequencies are then separated from the fundamental component through the demodulation, by finding the envelope. The pre-processed signals are converted into image representations for classifier training using a convolutional neural network. Unlike the original method in [11] that employs computationally expensive scalograms, this paper proposes using more efficient recurrent graphs, achieving comparable diagnostic accuracy with significantly reduced computational requirements.

The recurrence graph is defined as a binary matrix  $R$ , where each element  $R_{i,j}$  is determined by:

$$R_{i,j} = \Theta(\varepsilon - \|x_i - x_j\|), \quad i, j = 1, \dots, N,$$

where  $N$  is the number of measured points  $x_i$ ,  $\varepsilon$  is a threshold distance,  $\Theta(\cdot)$  is the Heaviside step function and  $\|\cdot\|$  is a norm. The matrix  $R$  is symmetric across its main diagonal and highly sensitive to the  $\varepsilon$  threshold selection.

An alternative approach uses a distance matrix  $D$  with elements

$$d_{i,j} = \|x_i - x_j\|,$$

eliminating threshold dependence. To convert these distances into grayscale images, values are normalized to  $[0, 255]$  by computing the matrix's minimum and maximum values. The resulting

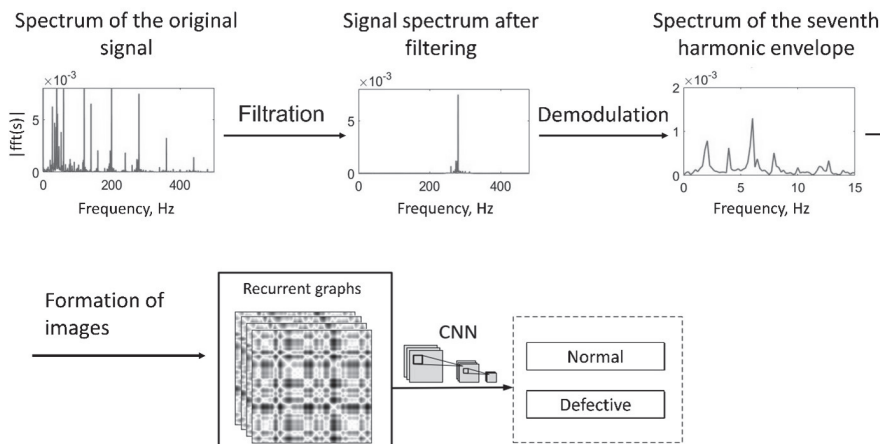


**Fig. 1.** Scheme of the proposed method.

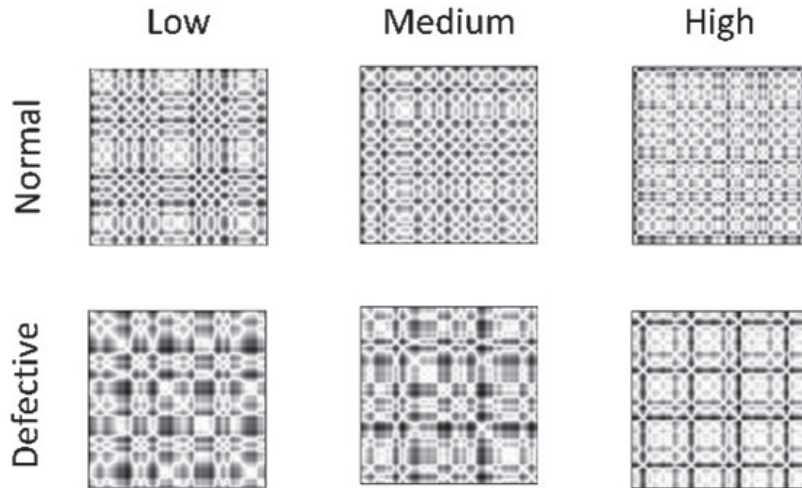


**Fig. 2.** Recurrence graphs of signals for healthy and rotor-bar-faulty induction motors under low, medium, and high load conditions.

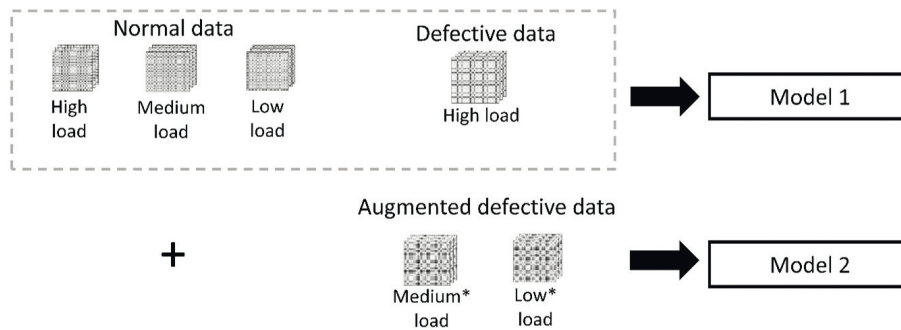


**Fig. 3.** Training datasets using only original data (Model 1) and augmented data (Model 2).

images are resized to  $256 \times 256$  pixels using linear interpolation, which scales the original data to the target resolution while preserving value transitions.

Figure 2 displays  $256 \times 256$  pixel recurrence plots generated from signals representing different motor operating conditions. The underlying dataset used to produce these images will be comprehensively detailed in Section 4. The analysis of the generated recurrence plots reveals two key findings. First, the visible dissimilarities between plots from healthy and defective motors confirm that the model can effectively differentiate between these operational states. Second, the observed variations across different operating modes suggest potential challenges for model generalization, particularly when processing data from the operating conditions that were not represented in the training dataset.

In practice, limited data availability across load conditions restricts the model's classification accuracy. While healthy motor signals can be acquired under various operating modes, faulty motor data is typically available for only one load condition. Consequently, the training set contains defect patterns from a single operating mode, constraining model performance. This scenario corresponds to Model 1 in Fig. 3.

To address this limitation, we propose augmenting the dataset through load simulation. By artificially generating signal variations that emulate different load conditions, we can significantly expand the available training data for faulty motor states. Model 2 (Fig. 3) trained on such a data

set will have greater load invariance, which will improve its accuracy in classifying different motor states. The method of current signal augmentation to expand the faulty data set will be described in the next section.

### 3. DFT SPECTRUM RESTRUCTURING METHOD FOR DATA AUGMENTATION

The  $N$ -point Discrete Fourier Transform (DFT)  $S(k)$  of a discrete signal  $s(n)$ ,  $n = 0, \dots, N - 1$ , is given by:

$$S(k) = \sum_{n=0}^{N-1} \left( s(n) e^{-j \frac{2\pi nk}{N}} \right), \quad k = 0, \dots, N - 1,$$

where  $j$  is the imaginary unit.

The signal  $s(n)$  can be recovered from its DFT by taking the inverse DFT:

$$s(n) = \frac{1}{N} \sum_{k=0}^{N-1} \left( S(k) e^{j \frac{2\pi nk}{N}} \right), \quad n = 0, \dots, N - 1.$$

The DFT of a real-valued signal has the following conjugate symmetry property:

$$S(N - m) = S^*(m), \quad m = \begin{cases} 1, \dots, \frac{N}{2} - 1, & \text{if } N \text{ is even,} \\ 1, \dots, \frac{N-1}{2} - 1, & \text{if } N \text{ is odd.} \end{cases}$$

Here  $*$  denotes the complex conjugation operation.

The complex-valued discrete function  $S(k)$  can be written in exponential form:

$$S(k) = A(k) e^{j\Phi(k)},$$

where  $A(k) = |S(k)|$ ,  $\Phi(k) = \arg S(k)$  are known as the amplitude spectrum and the phase spectrum, respectively.

From the property of complex symmetry  $S(N - m) = S^*(m)$  for real-valued signals, the symmetry properties follow:

$$A(N - m) = A(m), \quad \Phi(N - m) = -\Phi(m).$$

Our method involves stretching (or compressing) the original spectrum on the interval  $[a, c]$  to a new interval  $[a, c_1]$ , while compressing (or stretching) the spectrum on  $[c, b]$  to  $[c_1, b]$ . This transformation modifies the spectral segment  $S(k)$  over  $[a, b]$ , corresponding to frequency range  $\left[ \frac{a \cdot Fs}{N}, \frac{b \cdot Fs}{N} \right]$ , where  $Fs$  is the sampling frequency. Due to spectral symmetry requirements, it is also necessary to change the corresponding symmetric parts of the spectra.

For spectral transformation, we employ linear interpolation. Given that  $S(k)$  is the complex-valued function, we can either interpolate its real and imaginary parts, or interpolate its magnitude and its argument. These two approaches can lead to different results. For example, the work [12] examines these different approaches to interpolating complex response amplitude operator data which are used in marine hydrodynamics for the prediction of the ship motions. Interpolation of complex numbers using the real and imaginary parts performed worst for most cases tested in [12]. The authors also used linear interpolation and stated that it is "safest" to use as it ensures interpolated values will always be within the ranges of neighboring values.

Our experiments have convinced us that for our problem, linear interpolation using separate interpolation of the magnitude and the argument, rather than real and imaginary parts, is preferable. This interpolation is used in the spectrum distortion algorithm proposed below.

**Algorithm 1** (of spectrum distortion).

$[a, c] \rightarrow [a, c_1], [c, b] \rightarrow [c_1, b]$  :

Input:  $s(n), Fs, a, b, c, c_1$ .

1) Calculate DFT  $S(k)$  of  $s(n)$ .

2)  $[a, c] \rightarrow [a, c_1]$ :

2.1) Calculate the stretching rate:  $p = \frac{c_1 - a}{c - a}$ .

2.2) Old samples:  $t = 0 : \frac{1}{Fs} : \frac{c - a}{Fs}$ .

2.3) New samples (the interpolation nodes):  $t_1 = 0 : \frac{1}{p \cdot Fs} : \frac{c - a}{Fs}$ .

2.4) Part of the spectrum to be distorted:  $u = S(a : c)$ .

2.5) Interpolate separately the magnitude and argument of  $u$ :

$$\hat{u} = \text{interp}(t, |u|, t_1) \cdot \exp(j \cdot \text{interp}(t, \arg u, t_1))$$

3)  $[c, b] \rightarrow [c_1, b]$ :

3.1) Calculate the stretching rate:  $p = \frac{b - c_1}{b - c}$ .

3.2) Old samples:  $t = 0 : \frac{1}{Fs} : \frac{b - c}{Fs}$ .

3.3) New samples (the interpolation nodes):  $t_1 = 0 : \frac{1}{p \cdot Fs} : \frac{b - c}{Fs}$ .

3.4) Part of the spectrum to be distorted:  $v = S(c : b)$ .

3.5) Interpolate separately the magnitude and argument of  $v$ :

$$\hat{v} = \text{interp}(t, |v|, t_1) \cdot \exp(j \cdot \text{interp}(t, \arg v, t_1))$$

4) Concatenate:

$$W = [\hat{u}(1 : \text{end} - 1), \hat{v}(1 : \text{end})] \text{ or } W = [\hat{u}(1 : \text{end}), \hat{v}(2 : \text{end})].$$

5) Initialize  $\hat{S}(k) = S(k)$ .

6) Replace the desired part with the interpolated one:  $\hat{S}(a, b) = W$ .

7) Take into account the property of spectrum symmetry:

if  $a \neq 0$

$$\hat{S}(N - b - 1 : N - a - 1) = (\text{flip}(W))^*,$$

else:

$$\hat{S}(N - b - 1 : N - a) = (\text{flip}(W(2 : \text{end})))^*,$$

Output: distorted DFT  $\hat{S}(k)$

*Remark 1.* In step 4 of the Algorithm, it is necessary to take into account that one and the same sample  $c$  is included in both  $\hat{u}$  and  $\hat{v}$ , so it should not be taken twice.

*Remark 2.* The case  $a = 0$  needs to be considered separately, because  $S(0)$  lacks a symmetric counterpart in the spectrum.

*Remark 3.* *flip* reverses the order of the elements. *interp*( $t, f, t_1$ ) returns interpolated values at points  $t_1$  of a function  $f$  initially given by its values at points  $t$ .

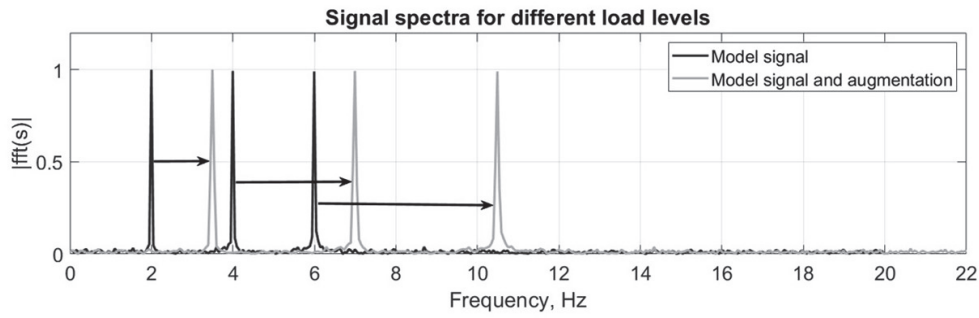


**Fig. 4.** Spectrum restructuring to obtain a signal with frequencies corresponding to a high load.

Let us consider the application of the algorithm using the following example. We model the envelope of the signal from a faulty rotor, containing three equally spaced frequencies of 2, 4, 6 Hz.

$$s(t) = \sum_{k=1}^3 \cos(2\pi f_1 t \cdot k) + n(t),$$

where  $f_1 = 2$  Hz, and  $n(t)$  is the additive Gaussian noise. The Signal-to-Noise Ratio (SNR) was measured at 16 dB, calculated as:

$$\text{SNR} = 10 \log_{10} \left( \frac{P_s}{P_n} \right),$$

where  $P_s$  and  $P_n$  represent the signal power and noise power, respectively. The signal duration was 4 seconds with a sampling frequency  $F_s = 50$  Hz, yielding  $N = 200$  samples.

According to the algorithm, we take:  $a = 0 \cdot \frac{N}{F_s}$ ,  $b = 20 \cdot \frac{N}{F_s}$ ,  $c = 8 \cdot \frac{N}{F_s}$ ,  $c_1 = 14 \cdot \frac{N}{F_s}$ . Here the  $\frac{N}{F_s}$  multiplier is used to go from frequency to sample number. Thus, we modify the spectrum in the section from 0 Hz to 20 Hz as follows. We stretch a part of the spectrum in the frequency range [0, 8] Hz to a new range [0, 14] Hz, and compress a part in the range [8, 20] Hz to [14, 20] Hz. Under this transformation, the original equispaced frequencies (2 Hz, 4 Hz, 6 Hz) are mapped to new equispaced frequencies (3.5 Hz, 7 Hz, 10.5 Hz). The spectra of the original and restructured signal are shown in Fig. 4. As expected, the spectra are identical above 20 Hz since this frequency region remained unmodified by the transformation.

In induction motors, the characteristic peak spacing in the envelope spectrum equals  $2s$ , where  $s$  is the motor slip coefficient. Our simulation of frequency transformation from (2, 4, 6) Hz to (3.5, 7, 10.5) Hz effectively models a slip change from 1 to 1.75 caused by a change in the motor load.

#### 4. EXPERIMENTAL DATA

The effectiveness of the proposed diagnostic method was studied using data obtained from an experimental setup, which includes a 0.37 kW induction motor with one pair of poles, a bearing shaft connected to the motor through a claw coupling, a belt drive and a load. The load is a brake with permanent magnets that sets the torque on the motor shaft. A frequency converter powers the motor and sets the rotor speed.

The study utilized two identical motors: one healthy and one with artificially induced rotor bar defects (three drilled holes in the bar area). Stator current data was collected across supply frequencies from 20 Hz to 50 Hz (10 Hz increments) under three load conditions: Low (2%), Medium (20%), and High (36%) of rated torque. For each load level, four 60-seconds signals were recorded

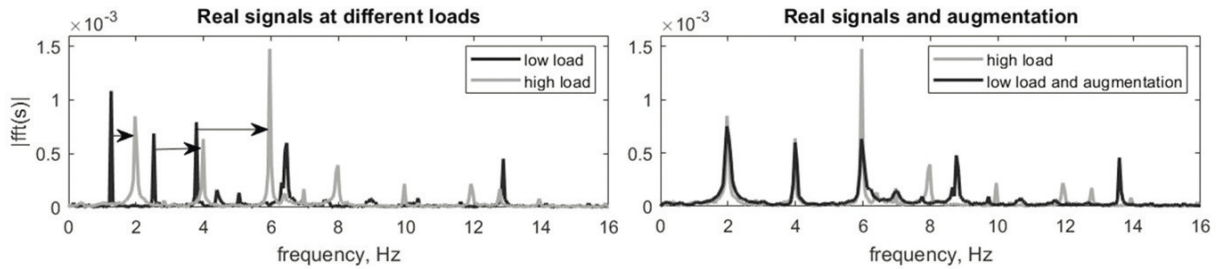


**Fig. 5.** Current signal spectra for low and high load levels (left — both signals are real, right — light — real, dark — synthetic).

at 50 kHz sampling frequency. The training set for Model 2 augmented real fault data using the spectral restructuring method described previously.

Figure 5 displays envelope spectra of actual current signals under two load conditions. Defect-related spectral peaks appear at: 1) low load (2%): 1.2 Hz, 2.4 Hz, 3.6 Hz; 2) high load (36%): 1.9 Hz, 3.8 Hz, 5.7 Hz. Through spectral restructuring, we transform the low-load signal by stretching the  $[0, 4.8]$  Hz interval to  $[0, 7.6]$  Hz. The spectrum of the new, rebuilt signal (Fig. 5, right), closely matches the actual high-load spectrum. Since there are no signals at different load levels in real conditions, our method allows compensating for the lack of data by creating them synthetically.

## 5. EXPERIMENT RESULTS

The training sets for Model 1 and Model 2 each contained 3000 recurrence plot representations ( $256 \times 256$  pixels) derived from processed current signals. The training approach differed between models: Model 1 used only high-load fault data, whereas Model 2 combined real high-load data with augmented samples (Fig. 6). For testing the trained Models 1 and 2, a set containing 1000 images for each class and for each load was used.

The training dataset consists of 1500 images for each class. The normal class contains data for all load values. In the case of Model 1, the defective class contains 1500 images of signals obtained at one load level. In the case of Model 2, the defective class contains 500 images of real signals obtained at the same load level as for Model 1 and 1000 images of synthetic signals obtained by augmentation, i.e., also 1500 images in total.

For training purposes, we utilize fault data collected under high-load conditions, as this operational regime represents the most critical and industrially relevant case, given that equipment

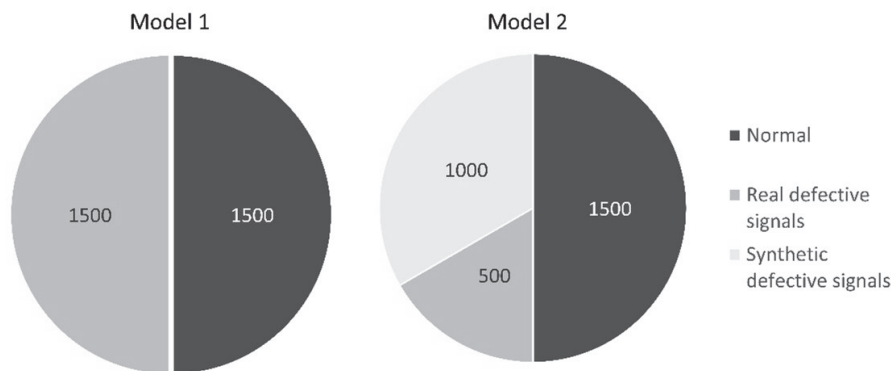


**Fig. 6.** Composition of the training dataset for Model 1 and Model 2.

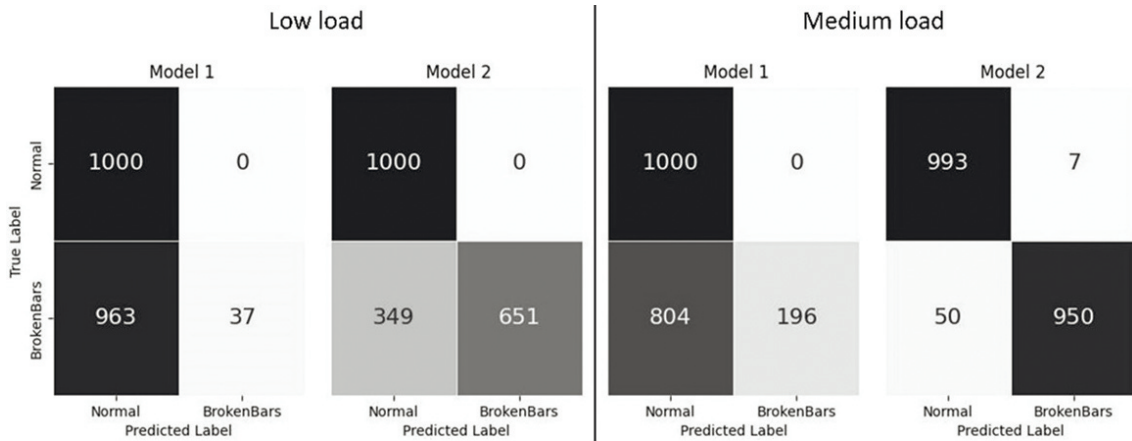


**Fig. 7.** Confusion matrices for Model 1 and Model 2.

typically operates under substantial loads. The model's capability to identify faults under low-load conditions demonstrates its sensitivity, as these subtle signatures are particularly challenging to detect. This example specifically evaluates the model's performance in recognizing incipient faults during their early developmental stage.

A 9-layer neural network model is used to train on the generated image dataset. The first 2D convolution layer includes 32 kernels that produce  $256 \times 256$  feature maps. The next pooling layer performs the pooling operation, producing 32 maps of size  $128 \times 128$ . The second convolution layer generates 64 maps of size  $128 \times 128$ . This is followed by another pooling layer that produces 64 maps of size  $64 \times 64$ . The third convolution layer produces 128 maps of size  $64 \times 64$ , and the next pooling layer generates 128 maps of size  $32 \times 32$ , which are then pulled out and fed to a fully connected layer with 2048 neurons. At the output, the data is passed through two additional fully connected layers and an output layer.

Model 1 training was completed after 100 epochs. While demonstrating perfect (100%) classification accuracy on high-load test data, its performance on low-load conditions (Fig. 7) revealed limitations: though all normal-class images were correctly identified, only 37 defective samples were properly classified. Model 2 similarly achieved perfect (100%) classification accuracy on high-load test data. For low-load conditions, the model showed significantly improved performance, correctly identifying 651 defective-class images — representing an order-of-magnitude increase in detection capability compared to Model 1. Consequently, Model 1 achieved an average accuracy of 52% on low-load conditions, while Model 2 demonstrated significantly improved performance with 83% accuracy — a 31 percentage point increase in diagnostic capability.

On medium-load test data, Model 1 achieved 60% classification accuracy compared to Model 2's 98% accuracy, though Model 2 produced seven false positives. It is important to note that in real production environments, the focus is usually on minimizing false negative cases, as they can lead to more serious consequences. Therefore, false positive classification errors are considered less critical for Model 2.

## 6. CONCLUSION

The paper proposes a method for diagnosing a broken rotor bar of an induction motor under realistic industrial conditions characterized by limited fault data availability. To solve the problem of insufficient training sample, we introduce a novel signal augmentation technique based on spectral restructuring. This approach allows modeling variations in the motor load, generating synthetic signals corresponding to both a decrease and an increase in load, which expands the representativeness of the data set.

This work also introduces, for the first time, the application of recurrence plots for induction motor fault diagnosis as an effective time-series visualization and analysis tool. Compared to conventional color scalograms requiring wavelet transform computation, recurrence plots offer superior computational efficiency while preserving feature discriminability. This allows reducing computational costs without losing classification accuracy.

During the experimental studies, it was found that the use of a convolutional neural network trained on recurrent graphs, in combination with the developed data augmentation method aimed at modeling reduced load conditions, led to a significant increase in the accuracy of defect classification. The achieved performance improvement validates the augmentation approach's effectiveness in developing load-invariant fault detection models.

The proposed methodology — combining spectral-based synthetic data generation with recurrence plot analysis — significantly enhances diagnostic reliability under data scarcity conditions. These findings directly support the development of robust predictive maintenance systems for industrial induction motors, particularly in scenarios with limited fault examples available for training.

#### FUNDING

This work was financially supported by Ministry of Science and Higher Education of the Russian Federation (FENU-2023-0010).

#### REFERENCES

1. Zadirán, K.S. and Shcherbakov, M.V., Forecasting Rare Events in the Evaluation of Equipment Residual Life, *Automation in Industry*, 2024, no. 10 pp. 10–15.
2. Kryukov, O.V., Intelligent Sensors for Predicting the Technical Condition of High-Voltage Electric Motors, *Automation in Industry*, 2013, vol. 10, pp. 38–41.
3. Aleksandrov, A.I. and Kvaratskhelia, N.G., Monitoring and Forecasting the Technical Condition of Electric Motors, *Automation in Industry*, 2020, vol. 10, pp. 39–43.
4. Singh, G.K. and Al Kazzaz, S.A., Induction Machine Drive Condition Monitoring and Diagnostic Research—A Survey, *Elec. Power Syst. Res.*, 2003, vol. 64, no. 2, pp. 145–158.
5. Garcia, M., Panagiotou, P.A., Antonino-Daviu, J.A., and Gyftakis, K.N., Efficiency Assessment of Induction Motors Operating Under Different Faulty Conditions, *IEEE Trans. Ind. Electron.*, 2019, vol. 66, no. 10, pp. 8072–8081.
6. Lee, S.B. et al., Condition Monitoring of Industrial Electric Machines: State of the Art and Future Challenges, *IEEE Ind. Electron. Mag.*, 2020, vol. 14, no. 4, pp. 158–167.
7. Lighthill, M.J., Contributions to the Theory of Heat Transfer Through a Laminar Boundary Layer, *Proc. R. Soc. London. Ser. A. Math. Phys. Sci.*, 1950, vol. 202, no. 1070, pp. 359–377.
8. Lee, S.B. et al., Identification of False Rotor Fault Indications Produced by Online MCSA for Medium-Voltage Induction Machines, *IEEE Trans. Ind. Appl.*, 2016, vol. 52, no. 1, pp. 729–739.
9. Zhang, P., Du, Y., Habetler, T.G., and Lu, B., A Survey of Condition Monitoring and Protection Methods for Medium-Voltage Induction Motors, *IEEE Trans. Ind. Appl.*, 2011, vol. 47, no. 1, pp. 34–46.
10. Tang, J., Yang, Y., Chen, J., Qiu, R., and Liu, Z., Characteristics Analysis and Measurement of Inverter-Fed Induction Motors for Stator and Rotor Fault Detection, *Energies*, 2019, vol. 13, no. 1, p. 101.
11. Galshev, D.V., Development of a Method for Diagnosing Broken Bars in Induction Motors Using Current Signals, *Materials of IX All-Russian Youth Scientific Forum Science of the Future — Science of the Young*, Samara, 2024, p. 150.
12. Thornhill, E., Interpolation of Complex-Valued Response Amplitude Operators: Approaches and Effects, Defence Research and Development Canada — Atlantic Research Centre, November 2019, p. 77.